Zhou *et al. AAPPS Bulletin* (2022) 32:35
https://doi.org/10.1007/s43673-022-00064-1

AAPPS Bulletin

REVIEW ARTICLE

Open Access

Status of the high-intensity heavy-ion accelerator facility in China

Xiaohong Zhou*, Jiancheng Yang and the HIAF project team

Abstract

Nuclear physics has been aiming at understanding of the origin, structure, and property of strongly interacting matters, which constitute nearly all visible matter in the universe. Despite tremendous breakthroughs and achievements over the past century, there still exists overarching questions that animate nuclear physics today and incite constructing next-generation heavy-ion accelerator complexes worldwide. In order to promote the national development of heavy-ion science and technology, China government approved the high-intensity heavy-ion accelerator facility (HIAF) in 2015, proposed by the Institute of Modern Physics, Chinese Academy of Sciences. HIAF is composed of a superconducting ion linear accelerator, a high-energy synchrotron booster, a high-energy radioactive isotope beam line, an experimental storage ring, and a few experimental setups. By using HIAF characterized with unprecedented intense ion beams from hydrogen through uranium, we can produce a large variety of exotic nuclear matters not normally found on the Earth, including super-heavy nuclides, short-lived extremely neutron-rich and proton-rich nuclides, finite nuclear matters in the quantum chromodynamics phase diagram, exotic nuclides containing hyperons, meson-nucleus-bound systems, and highly charged ions. Therefore, HIAF will bring researchers to the forefront of promoting the most vigorous and fascinating fields in nuclear physics, such as to explore the limits to the existence of nuclides in terms of proton and neutron numbers, to discover exotic nuclear structure and properties and then to study the physics behind, to understand the origin of heavy elements in the cosmos, to depict the phase diagram of strongly interacting matter, etc. In addition, HIAF will provide an excellent platform to develop heavy-ion applications in life science, space science, and material science. The construction of HIAF started up in December of 2018 and takes 7 years. The civil engineering and infrastructure are being constructed on time schedule and will be completed in July, 2023. R&D on key accelerator techniques are going on successfully, and prototypes of core devices are fabricated in collaboration with home and abroad universities, institutes, and companies. Presently, we come to the stage of invitation for bids and volume production of various apparatuses. We plan to start facility installation in summer of 2023. As a scientific user facility opening to domestic and oversea researchers, HIAF user community plays key roles in defining research programs and raising requirements. We call upon expertise, aspirations, and resources of a host of collaborators. Collaborations, dedicated to specific research subjects, are established and will be established. These collaborations develop new experimental techniques and methods and take responsibility for design and building of measurement systems. We have completed the design of experimental setups. A new gas-filled recoil separator and a novel storage-ring-based isochronous mass spectrometer are already built, and other measurement systems are under construction. The facility commissioning is scheduled at the end in the year of 2025. After into operation of the 2.5 billion Chinese yuan HIAF, this world-class facility will ensure the nation's continued competitiveness in heavy-ion physics and technology through provision of outstanding discovery potential. Based on HIAF, we aim at establishing

*Correspondence: zxh@impcas.ac.cn

Institute of Modern Physics, Chinese Academy of Sciences, Lanzhou 730000, China

a world's leading laboratory for research and education in nuclear science, accelerator physics and technology, and applications of energetic heavy ions to meet societal needs. In this paper, progress and status of civil engineering and infrastructure construction of HIAF are introduced, R&D on critical accelerator techniques and prototypes of core devices as well as development of new experimental techniques and methods are presented, and design and construction of experimental setups and the associated physics research programs are briefly depicted.

Keywords: Heavy-ion accelerator, Heavy-ion beam, Super-heavy element, Radioactive isotope beam, Nuclear matter, Hypernuclide, Exotic nuclide, Nuclear mass

1 Introduction

The Institute of Modern Physics (IMP), Chinese Academy of Sciences, has built and operated the Heavy Ion Research Facility in Lanzhou (HIRFL), a national user facility opening to domestic and abroad researchers. Over a half century, HIRFL has been playing a leading role to develop heavy-ion accelerator techniques and to promote heavy-ion physics and applications in China. After the commissioning of the cooler storage ring of HIRFL in 2007, researchers at IMP had discussed the needs for a next-generation heavy-ion accelerator facility to produce intense ion beams. With great efforts, we had defined the scientific drivers and worked out the facility scheme. Chance came to us in 2010. In this year, China government decided to build a batch of Major National Science and Technology Infrastructure Facilities mainly dedicated to fundamental sciences and called for proposals nationwide. IMP proposed the project named as high-intensity heavy-ion accelerator facility (HIAF). Through a series of evaluations organized by the National Development and Reform Commission of China, HIAF project was officially approved in December of 2015, and IMP was charged to be responsible for the facility design and construction. After the assessment of technical feasibility, construction of HIAF started up on December 23, 2018 [1, 2]. HIAF is built in Huizhou City of Guangdong Province in South China. The construction lasts for 7 years, and the facility will be commissioned at the end of 2025. The total investment is 2.67 billion Chinese yuan, 1.67 billion yuan from the central government for facility construction, and 1.0 billion yuan from the local governments for civil engineering and infrastructure construction.

The basic idea of HIAF design is to couple a linear accelerator with a synchrotron to deliver ion beams from hydrogen through uranium with energies from MeV/u to GeV/u. We employ state-of-the-art accelerator techniques needed for producing intense ion beams. At HIAF, we can produce a large variety of exotic nuclear matters, including super-heavy elements and nuclides, extremely neutron-rich and proton-rich nuclides far away from the β-stability line, and finite high-density nuclear matters. In addition, we can also produce highly charged ions, exotic nuclides containing hyperons, meson-nucleus bound systems, and Δ-resonances in nuclear medium. Therefore, HIAF will be one of the world's leading heavy-ion accelerator complexes in the envisaged future. As a scientific user facility, we expect that researchers from all over the world can approach the experimental limits and open new domains of physics researches. The primary scientific goals of HIAF include the following:

To explore the limits to the existence of nuclides in terms of proton and neutron numbers as well as mass number

To discover exotic structure and properties in weakly bound nuclides and then to recognize the physics behind

To understand the origin of chemical elements particularly from iron through uranium in the universe

To search for the critical point in the quantum chromodynamics (QCD) phase diagram of strongly interacting matter

In addition, HIAF will play a leading role to promote heavy-ion applications in China. In collaboration with domestic institutions and companies, we will carry out applied basic researches and develop new radiation technologies to be applied in various fields. The major research subjects include production of medical isotopes, assessment of the single particle effects of chips and electronics used in space science, evaluation of materials applicable to advanced nuclear energy systems, mutation breeding of new crop varieties, and fabrication of nuclear track membrane. In heavy-ion applications, users seek for financial supports dedicated to building experimental setups. In this paper, the application research programs are not introduced.

Design and construction of HIAF provide great opportunities to train and grow up next generation of accelerator experts to fulfill critical workforce needs in accelerator fields, such as accelerator physics, advanced ion source technology, design and fabrication of superconducting magnets and cavities, radio frequency power engineering, large-scale cryogenic engineering, intense ion-beam control and diagnosis technology, etc. HIAF

user community, through delivering scientific discoveries and developing heavy-ion applications, educates young scientists who will advance the benefits and knowledge of nuclear science and technology for generations to come. Therefore, HIAF will play a key role for sustainable development of heavy-ion science and technology in China. As a scientific user facility, an international research center of heavy-ion science and technology will be created on the basis of HIAF.

2 Progress of civil engineering and infrastructure construction

HIAF is a completely new facility, and it is built on a primordial place without any existing infrastructure. A flat space of about 2 km^2 was prepared by cutting hills to backfill ditches, where HIAF is being built. A water supply system and an electricity supply station with distribution powers of 80 MW@380 V and 32 MWs@10 kV are already built. Two cryogenic stations are under construction, which will provide circulatory liquid helium flow to sustain superconducting magnets and cavities. To shield radiations induced by energetic ions, the whole facility is laid 12.6 m below ground level. The 1700 m tunnel housing HIAF is generally 6.8 m in height and 8.0 m in width, but at specific positions, spaces are enlarged for installation of large-scale apparatuses. The tunnel and experimental halls will be set up at the end of 2022. Ground buildings are under construction. Figure 1 shows the construction site as of August 2022. It is scheduled that civil engineering and infrastructure construction will be completed in summer of 2023, and then, we will switch to facility installation.

We have developed the SolidWorks software, by which all components of the accelerator system and the experimental setups as well as the complicated pipe and cable networks are integrated together and the layouts are optimized. A 3D model of a virtual HIAF is built. Building information modeling (BIM) is utilized generally by civil engineers for structural analysis in large-scale constructions. BIM has the functions of integration, drawing, visualization, etc. Revit is a popularly used software of BIM, but it is incompatible with mechanical design software such as SolidWorks. We add mechanical designs into the civil engineering 3D drawing of Revit and hence build a complete engineering model for HIAF project. Using this model, we integrate the buildings, the accelerator system and experimental setups, and the auxiliary support systems. Therefore, exact position of each device and its connection with others can be determined precisely, which makes facility installation efficiently. This development has a great significance for construction, maintenance, and upgrade of HIAF.

HIAF location is far away from the campus of IMP. In order to facilitate the construction and management, a new branch of IMP was built in Huizhou City and into service at the beginning of 2022. Engineers, technicians, and researchers move to there from the institute according to the project schedule.

3 Accelerator complex and R&D on key accelerator techniques

3.1 Brief introduction to the accelerator complex of HIAF

HIAF is a large-scale heavy-ion research facility. As shown in Fig. 2, it is composed of the ion sources, the

Fig. 1 Photo of HIAF construction site taken by an unmanned aerial vehicle in August of 2022. The profile of HIAF is visible. The China ADS facility is under construction on the same campus, located in the left area of the platform

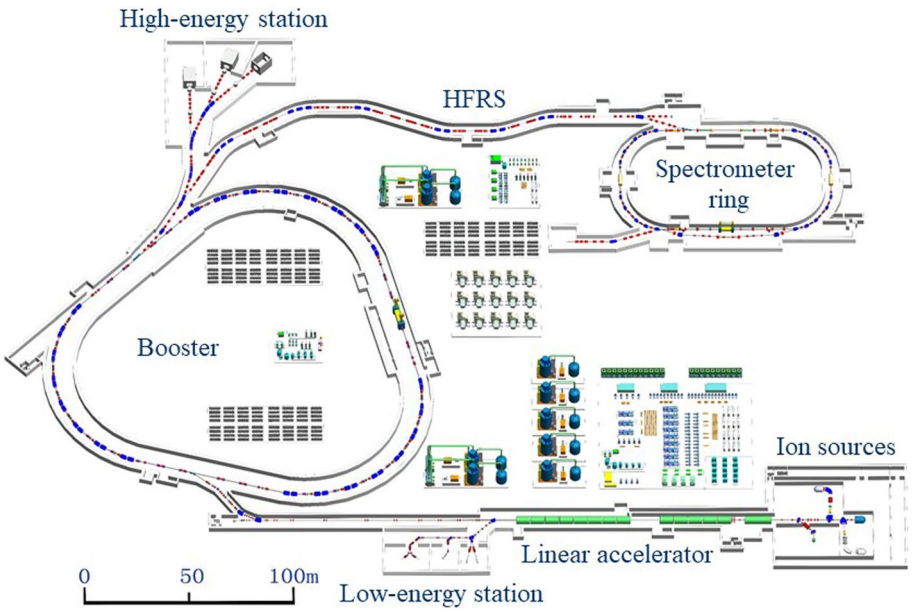

Fig. 2 Layout of HIAF. The major sub-systems are sketched, including the ion sources, the superconducting ion linear accelerator, the high-energy synchrotron booster, the high-energy fragment separator, and the experimental spectrometer ring. The low-energy and high-energy experimental stations are also indicated

superconducting ion linear accelerator (hereafter abbreviated as linear accelerator), the high-energy synchrotron booster (booster), the high-energy fragment separator (HFRS), the experimental spectrometer ring (spectrometer ring), and the experimental setups.

The linear accelerator with a length of 114 m is equipped with three ion sources, including a new-generation 45 GHz, 20 kW superconducting ECR (electron cyclotron resonance) ion source. It can be operated with either a continuous-wave (CW) mode or a pulse mode, providing intense beams for low-energy experiments or injecting ions into the booster, respectively. The linear accelerator is able to deliver 1.0 emA beams with mass number to charge number ratio of $A/Q = 2 \sim 7$ in pulse mode or 10 pμA beams with $A/Q = 2 \sim 5$ in CW mode. $^{238}U^{35+}$ beam can be accelerated to a maximum energy of 17 MeV/u. The booster with a circumference of 569 m and a maximum magnetic rigidity of 34 Tm accumulates and stores huge ion number under a large phase-space condition. Due to space charge and dynamic vacuum effects, ions stored are launched quickly to high energy employing a fast-ramping rate operation with a repetition rate of 3 Hz. HFRS coupled to the booster produces unstable nuclides via projectile fragmentations or in-fight fissions of heavy projectiles and then separates, identifies, and transports the nuclides of interest for various experiments. With slow extraction mode of the booster, HFRS works as a separator and spectrometer. With fast extraction mode, HFRS injects highly charged ions from the booster or reaction products into the spectrometer ring for storage-ring-based experiments. In addition, slowly extracted beams can be delivered to the high-energy experimental station.

Typical beams from the booster are presented in Table 1. We can see that very intense ion beams will be available. The intensities shown are obtained by optimizing the charge state of the ions, i.e., they are the highest intensities for the specific isotopes. Taking ion of $^{238}U^{35+}$ as an example, about 1.0×10^{11} particles with a maximum energy of 835 MeV/u can be stored in the booster. ^{238}U beam can be accelerated to higher energy using higher charge state if needed on a trade-off of

Table 1 Typical beams from the booster. The beam intensities are given in the unit of particles per pulse (ppp)

Ion species	Energy (GeV/u)	Intensity (ppp)
p	9.3	2.0×10^{12}
$^{18}O^{6+}$	2.6	6.0×10^{11}
$^{78}Kr^{19+}$	1.7	3.0×10^{11}
$^{209}Bi^{31+}$	0.85	1.2×10^{11}
$^{238}U^{35+}$	0.835	1.0×10^{11}

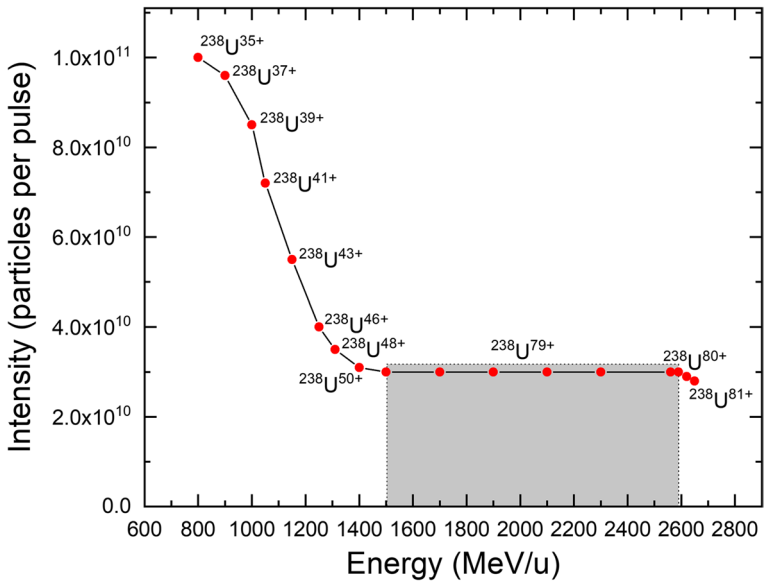

Fig. 3 Intensity-energy diagram of ^{238}U beam stored in the booster. The red dots represent the maximum particle numbers stored at the corresponding charge states

the beam intensity. We simulated the intensity-energy diagram of ^{238}U beam by changing its charge state. As shown in Fig. 3, the particle number of ^{238}U stored in the booster can be still as high as around 3×10^{10} if increasing the beam energy up to 2.6 GeV/u. Of course, higher beam energies are achievable for other kinds of beams. In slow extraction mode, quasi-continuous beams with a typical duration of 3 s are provided by using the third-order resonance and RF-knockout scheme. The stored particles are uniformly distributed in the beam duration. The designed spiral step at the entrance of the electrostatic septum is about 12 mm with low particle density near the wires for reducing head-on loss, and the Hardt condition is fulfilled with a horizontal chromaticity close to zero. The angular spread of extracted separatrices is minimized for reducing side-hit loss on blade. Therefore, slow extraction efficiency of more than 95% can be achieved.

We have calculated production yields of nuclides using projectile fragmentation, in-flight fission of heavy projectiles, multi-nucleon transfer, and fusion reactions. The optimal yield for each nuclide was presented previously [2]. Roughly, over 5000 species of nuclide can be produced with least production rate of one nuclide per day at HIAF, and consequently, we are able to access the proton drip-line nuclides up to uranium and extremely neutron-rich nuclides in medium and heavy mass regions. Therefore, HIAF will be one of the most powerful facilities in the world to explore the hitherto unknown territories in nuclide chart.

3.2 R&D on key accelerator techniques

Owing to the construction and operation of HIRFL comprising two cyclotrons and two storage rings, our institute has solid technical strengths to design and build a next-generation heavy-ion accelerator facility. The design and engineering team of HIAF is well organized, which constitutes specialized groups of accelerator physics and techniques. In past years, great efforts have been devoted to R&D on critical accelerator techniques. In collaboration with home and abroad institutions and companies, we have developed intense beam physics and technique and designed and fabricated prototypes of core devices.

The ion source front end should provide solutions to the stringent needs of the linear accelerator capable of accelerating intense beams with broad A/Q ratios. The ion sources and associated beam lines are sketched in Fig. 2, delivering high-quality beams to the downstream RFQ. We adopt a 45 GHz next-generation ECR ion source FECR (the first 4th-generation ECR ion source), a 24 ~ 28 GHz SECRAL (superconducting ECR ion source with advanced design in Lanzhou), and a 2.45 GHz intense beam ECR ion source. With the compact 2.45 GHz ECR ion source featuring permanent magnet structure and reliable beam production [3], we can produce over 2 mA H_2^+ and 1 mA H_3^+ CW beams. SECRAL has been well established and operated at HIRFL [4]. Intense highly charged beams are extracted from SECRAL, such as 300 eμA U^{35+} and 680 eμA Bi^{31+} beams [4], which make SECRAL one of the best performing ECR ion sources.

In order to attain the beam intensities list in Table 1 from the booster and the high beam intensities with the linear accelerator, very intense ion beams should be delivered from an ion source. The requirements are beyond the capacities of the state-of-the-art ECR ion sources. Therefore, we will build a 45 GHz FECR as shown in Fig. 4. The novel design can provide the conditions to produce and confine over 2.5 times hot and dense plasma compared to that of the 3rd-generation ECR sources, which is crucial for production of the desired beam intensities. It is expected that pulsed 50 pμA $^{238}U^{35+}$ beam with a duration of ~1 ms can be produced by FECR, which is 5 times higher than those delivered from existing ECR ion sources. There are many challenges in the development of FECR [5], of which the critical one is to fabricate a fully Nb_3Sn superconducting ECR magnet with a B-minimum configuration. After extensive R&D work [6], we fabricated the Nb_3Sn high-field superconducting magnet, the quasi-optical 45 GHz gyrotron microwave system, the beam extraction system, and the high-power aluminum plasma chamber with micro-channel cooling structure. At present, the components are in place for final assembly, and we expect the first plasma at 45 GHz in 2023.

The linear accelerator consists of a radio frequency quadrupole, a low-energy beam transportation system, and a superconducting section [7]. The superconducting section comprises 17 cryomodules with two types of accelerating structure, which can accelerate $^{238}U^{35+}$ ions to a maximum energy of 17 MeV/u. Each of the first 6 cryomodules contains 5 superconducting solenoids and 5 superconducting quarter-wave resonant cavities with β-value of 0.052 and working frequency of 81.25 MHz. Each of the successive 11 cryomodules is composed of 2 superconducting solenoids and 6 superconducting half-wave resonant cavities with β-value of 1.15 and working frequency of 162.2 MHz. We have designed the cold mass support, the liquid helium circulatory system, the cooling system, and the cooling coupler. The prototypes of cryomodule are assembled and now under test.

The booster is a normal conducting magnet ring comprising 48 dipole magnets, 78 quadrupole magnets, 30 sextupole magnets, and 80 correctors. Over half of the dipole magnets are manufactured and tested. The static magnetic field is proved with a high uniformity of $\pm 2.0 \times 10^{-4}$ in the full range of magnetic field from 0.047 to 1.58 T in a wide good field region, which is better than the design specification. The other magnets are under construction.

The booster is designed to store $^{238}U^{35+}$ ions up to 1×10^{11} particles. To overcome space charge limits, a transverse phase-space painting injection will be implemented for beam accumulation. In the painting injection scheme, the closed orbit changes over time with the horizontal and vertical injection bumps. Unlike the injection using charge exchange method implemented in proton machines, a tilted corner septum is employed for both transverse phase places of injection

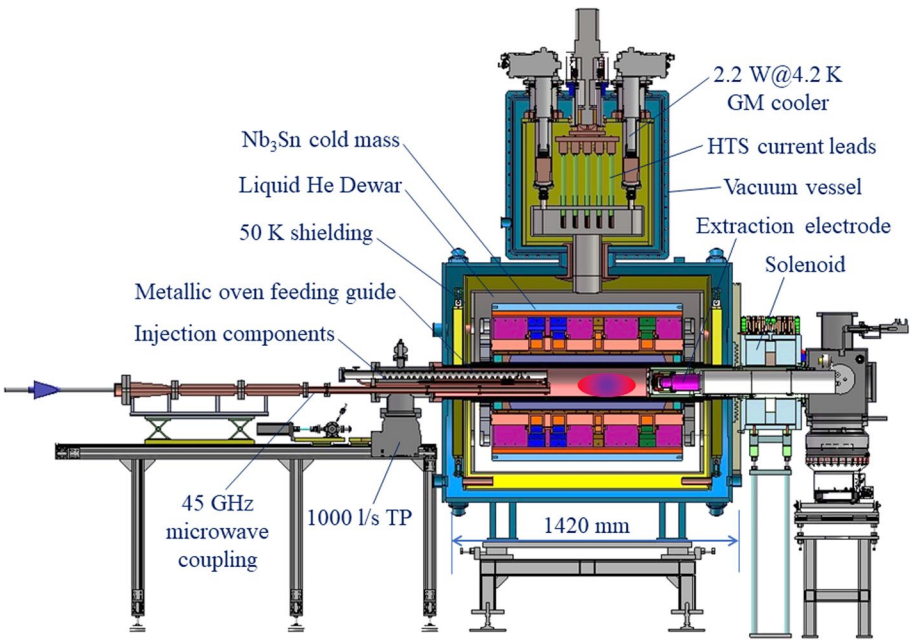

Fig. 4 Structure of FECR with major components indicated

simultaneously. Low loss and low phase-space dilution are basic requirements. Injection begins with horizontal and vertical bumps close to the centroid of injection beam and then gradually move away from it. Both the horizontal and vertical emittances are painted from small to large [8]. We have simulated the injection with $^{238}U^{35+}$ ions at an initial energy of 17 MeV/u, and it shows that an injection efficiency higher than 95% can be attained within 60 turns.

Due to space charge and dynamic vacuum effects, ions stored in the booster are launched to high energy quickly using a fast-ramping rate operation. A ramping rate of 12 T/s for the dipole magnets is needed for optimizing the space charge limits and collimators. Therefore, a power supply with a rising rate of 38 kA/s and a maximum current of 4 kA should be adopted for the dipole magnets. A full-energy-storage, fast-cycling pulse power supply is developed successfully. The test results show that the output of 3900 A/3 Hz with a rising rate 40,000 A/s and a tracking error of $\pm 9.6 \times 10^{-5}$ is achieved, which already meets the design specifications. A magnetic alloy acceleration cavity with a high accelerating voltage up to 240 kV is used to boost the energy of ions stored during fast-ramping operation. The cavity shown in Fig. 5 is built, and it is equipped with a 500 kW RF power source and a low-level control system.

Fast ramping of the magnets induces eddy currents in the vacuum chamber wall, which can cause distortion of magnetic fields. Ceramic-lined thin-wall vacuum chamber is a good solution to reduce the eddy current effect. The vacuum chambers are made of stainless steel with a thickness of 0.3 mm. To withstand the atmospheric pressure, the thin wall of vacuum chamber is supported by ceramic rings inside. The ceramic rings are made by yttrium-stabilized zirconia, which has very good mechanical strength and toughness. The ceramic rings are coated with a 1.0 μm gold film to reduce beam impedance and desorption rate of the ceramic surface. Compared to the chamber with reinforced ribs, the gap size of the dipole magnets decreases significantly. A prototype of the vacuum chamber has been built and tested in vacuum of 1.07×10^{-9} Pa, which basically meets the requirement.

The second stage of HFRS comprises superconducting dipole magnets and multipole magnets. It is the first time for us to make superconducting multipole magnets. An octupole coil, winded by ϕ2.0 mm six-round-one SC cable, is placed in the inner G10 mandrel. A quadrupole coil surrounding the octupole one is winded by ϕ2.8 mm six-round-one SC cable. The multipole magnet is encapsulated in an aluminum shell and impregnated inside liquid helium. A prototype of the multipole superconducting magnet is assembled. The quadrupole coil is charged with a 427 A current after two times of cooling-down and warm-up cycles, which is about 92% of the designed current.

The magnets of HFRS work in an extremely high radiation environment, and therefore, radiation-resistant techniques are adopted. The coils of the radiation-resistant magnets have saddle-type structure to avoid the intense radiation areas, and these coils are impregnated with radiation-resistant epoxy which can bear radiation doses up to 20 MGy. Additionally, radiation-resistant water pipes are used for these magnets instead of traditional rubber water pipes, which consist of copper tube, ceramic insulation, and metallic joints. It is estimated that the production target and beam dumps of HFRS accumulate extremely high radioactivity. After 1 month of continuous irradiation, the residual dose rate on the surface of these components can reach over 10^7 μSv/h. Thick steel shielding blocks are placed above the vacuum chambers of the production target and beam dumps to protect nearby radiation-sensitive devices such as cameras and motors from damage caused by prompt radiation. In the high radiation area, remote operations are implemented.

Fig. 5 Left, the magnetic alloy acceleration cavity. Right, the cavity coupled to a power source under test in a vacuum of 5.5×10^{-12} Pa

While developing new techniques and making prototypes of core devices, we have designed various instruments and equipments with proven technologies, such as normal magnets and power supply systems, high-vacuum systems, electron cooler, stochastic cooling device, beam monitors and diagnostic apparatuses, and hardware of machine protection system.

R&D and design work approach to the end, and now we turn to mass production.

4 Experimental setups and the related physics programs

4.1 Low-energy experimental station

The limits to the existence of nuclides in terms of proton and mass numbers are determined by the probability of spontaneous fission. If the fission barrier vanishes, the nuclide loses its stability against fission. In a liquid-drop model, it was predicted that nuclides with $Z > 103$ could not survive from spontaneous fission [9]. However, nuclides have shell structure manifested as a nonuniformity in the energy distribution of individual particle states near the Fermi level, which is directly connected to nuclear binding energies [10]. In 1960s, the approach of shell-effect correction to liquid-drop nuclear masses was developed [11], named macroscopic–microscopic approach. Soon later, this approach predicted the island of stability centered around a double-magic ($Z = 114$, $N = 184$) nuclide [12]. Historically, the nuclides, whose stability and existence are attributed to nuclear shell effects, were named as super-heavy nuclides. This happens to be around the end of actinide elements, and therefore nowadays, we refer all elements from $Z = 104$ Rf onwards as super-heavy elements and the corresponding nuclides as super-heavy nuclides.

Synthesis of new elements and study of their chemical properties as well as exploration of the stability island of super-heavy nuclides have always been remaining as hot research topics and inspired extensive investigations both experimentally and theoretically [13–16]. The importance of the relevant researches includes the following: how many elements can exist? What are the chemical properties of super-heavy elements? Up to which element is the ordering scheme of Mendeleev's periodic table still valid? What are the maximum proton and neutron magic numbers? Are there stable or long-lived super-heavy nuclides? What do exotic structure and properties of super-heavy nuclides appear under extremely strong Coulomb fields? Over a half century, momentous achievements in synthesis of transuranium nuclides and elements have been attained. To date, elements with atomic number up to 118 have been discovered in laboratories [13–16], resulting in the completion of the seventh period of the periodic table of elements. However, very successful epoch of syntheses of super-heavy elements using the reactions of ^{48}Ca projectiles bombarding heavy actinide targets came to the end since there is no sufficient amount of target materials heavier than californium [13, 14]. In order to synthesize new elements beyond element 118, projectiles heavier than Ca must be used. Many attempts were made for producing elements 119 and 120 via fusion reactions, such as $^{50}\mathrm{Ti} + {}^{249}\mathrm{Bk}$, $^{50}\mathrm{Ti} + {}^{249}\mathrm{Cf}$, and $^{54}\mathrm{Cr} + {}^{248}\mathrm{Cm}$ [17]. Unfortunately, no new elements were discovered, and the upper limits of cross sections measured experimentally were significantly lower than those with ^{48}Ca beams [17]. Therefore, syntheses of new elements require substantially increased beam intensities.

Unique chemical properties were predicted theoretically for some super-heavy elements and their compounds [18]. Experimental verification can elucidate the influence of relativistic effects on chemical properties of super-heavy elements. At existing accelerator facilities, atoms of super-heavy elements are produced at extremely low rates, few atoms per hour down to atoms per day (even lower) for elements Rf through Og. The tiny production rates as well as short half-lives hinder the chemical study of super-heavy elements. In order to produce sufficient super-heavy atoms for chemical investigations, intense heavy-ion beams are needed.

The linear accelerator provides intense heavy-ion beams, as high as 10 pμA for all kinds of ion, and the beam energies are adjustable around the Coulomb barriers of interacting system. Therefore, new isotopes and elements can be produced using fusion reactions. The gas-filled recoil separator has been proven to be an ideal tool to separate and study nuclides produced in complete fusion reactions [19–21]. A new gas-filled recoil separator (SHANS2, spectrometer for heavy atoms and nuclear structure 2) was designed and built. It features with a large angular acceptance and a high transmission efficiency. A photo of SHANS2 is shown in Fig. 6. The ion optics and trajectory simulation of SHANS2 were presented in Ref. [22]. This separator has a magnetic configuration of $\mathrm{Q_vDQ_hQ_vD}$. Here, D denotes a dipole magnet; Q_h and Q_v stand for horizontally and vertically focusing quadrupole magnets, respectively. Helium gas is filled with a pressure of about 100 Pa in the vacuum chamber as a working gas. A differential pumping system, separating the high-vacuum beam pipeline from the separator, is installed in front of the target chamber. The maximum magnetic rigidity is designed to be 2.5 Tm, which is high enough for separation of nuclides produced in fusion reactions. A detection system including two multi-wire proportional counters and a position-sensitive silicon detector array is placed at the end. Presently, we test SHANS2 using well-known reactions at existing

Fig. 6 Photo of the new gas-filled recoil separator, SHANS2

accelerator to determine optimal gas pressure and transmission efficiency. In addition, a chromatographic apparatus for chemical investigation of super-heavy elements is under construction, and it will be connected to SHANS2 instead of the focal plane detector array.

We also plan to produce neutron-rich heavy nuclides via multi-nucleon transfer reactions, which are characterized by large energy dissipation and nucleon exchange between interacting nuclides. For an appropriate reaction system with beam energy above the Coulomb barrier, such as ^{238}U + ^{248}Cm, the projectile evolves to the doubly magic nuclide ^{208}Pb and transfers nucleons to the target. Consequently, neutron-rich heavy and even super-heavy nuclides can be produced [23, 24]. Presently, the reactions employing uranium projectiles and actinide targets would be practically the only way to assess neutron-rich super-heavy nuclides. However, due to the reaction mechanism, the products recoiling out the target have very broad distributions in kinematic energy, emitting angle, and charge state. It is a great challenge experimentally to separate the products of interest from huge unreacted projectiles and unwanted products. We have figured out conceptually a separator for separation and identification of multi-nucleon transfer reaction products, which consists of a rotating target system, a gas stopper, a sextupole ion beam guide, a RFQ cooler and buncher, an isobaric analyzer, and an isotopic analyzer [25]. The separator provides pulsed low-energy, high-quality neutron-rich beams with mass numbers identified and then distributes the beams to a multi-reflection time-of-flight mass spectrometer or a decay spectrometer.

At the low-energy station, we will synthesize new elements using fusion reactions, for instances, ^{54}Cr + ^{243}Am or ^{50}Ti + ^{249}Bk reactions for production of element 119 and ^{55}Mn + ^{243}Am or ^{50}Ti + ^{249}Cf reactions for element 120. In addition, a physical pre-separation of super-heavy elements of interest is made by SHANS2. Chemical properties of simple substance or some kinds of compound of super-heavy elements can be studied by using gas-phase or vacuum chromatographic methods. The multi-nucleon transfer reactions will offer us opportunities for observation of new neutron-rich super-heavy isotopes. If the production yields are sufficient, we can perform measurements of decay spectroscopy and hopefully obtain valuable information on the single particle states in super-heavy region. The neutron-rich isotopes are expected to be longer lived, and they are ideal samples for detailed studies of chemical properties of super-heavy elements.

4.2 High-energy experimental station

High-energy stable beams extracted slowly from the booster are delivered to the high-energy experimental station shown in Fig. 2. Primary ^{238}U beams with energy over 2.0 GeV/u and $A/Z = 2$ beams up to 4.25 GeV/u energy will be available. We will focus on discovery of new hypernuclides and study of nuclear matter properties, for which the beamlines and corresponding setups are sketched in Fig. 3. In this station, a beamline is kept for heavy-ion application.

4.2.1 Hypernuclear physics

One of the principal goals in nuclear physics is to understand nuclear force that holds nucleons together. Nucleons, including neutron and proton, are composed of three up and down quarks. Nuclear force results from

essentially the interactions between nucleons in nuclear medium, and its basic natures are now known to some extent. For an insight into nuclear force, especially at short range, a crucial approach is to increase the quark degrees of freedom in nuclear system, which is to put additional quarks other than up and down quarks into nucleons inside a nuclide. This can be realized by introducing a hyperon into nuclide. Hyperon is a type of baryon composed of three quarks, of which at least one is heavier strange quark. A Λ-hyperon consists of one up, one down, and one strange quark. The isospin excitation of Λ-hyperon produces the so-called Σ hyperons including Σ^+, Σ^0, and Σ^-. Ξ^0 and Ξ^- hyperons contain two strange quarks, and Ω^- hyperon has three strange quarks. A bound state constituting hyperon(s) and nucleons is referred as hypernuclide. Fundamental baryonic interactions can be probed by studying structure and decay of hypernuclides.

After the discovery of hypernuclide in 1953 [26], about 40 hypernuclides were observed by employing cosmic rays and various beams from accelerators [27, 28]. In most cases, hypernuclides are produced by converting one or two nucleons in stable nuclides into hyperons, and consequently, the isospin values of known hypernuclides are close to those of stable nuclides. The approach developed by the HypHI collaboration is unique, by which hypernuclides are produced through relativistic energy projectile fragmentations [29]. The basic idea is that high-energy projectiles break on a target, and then, the fragments capture hyperon produced in a hot participant zone of the collisions, forming a hypernuclide. Owing to the reaction mechanism, the produced hypernuclides have large neutron or proton excesses and proceed almost in the same direction and with nearly the same velocity as the projectiles. Thanks to a large Lorentz factor, hypernuclides survive longer and decay behind the production target, and hence, their half-lives can be determined from the distribution of flight length. In this approach, projectile energies should exceed 1.7 and 3.75 GeV/u for productions of Λ-hypernuclides and double-strangeness hypernuclides, respectively.

In the high-energy experimental cave, a dedicated setup for study of hypernuclides is under consideration in collaboration with RIKEN [29]. This setup includes a superconducting solenoid magnet and a dipole magnet, both with up to 2 T magnetic field. In front of the solenoid surrounding the production target, a system of vertex detectors comprising Si-strip detectors and scintillating fibers is placed for measuring the interaction point of projectile on target. A stack of drift chambers or gas electron multiplier detectors tracking light-charged particles is laid inside the solenoid magnet. A surrounding barrel composed of plastic scintillators, and resistive plate chambers are placed for measuring time-of-flight values, energy depositions, and hit positions of light charged particles. At the end, heavy charged particles are measured by resistive plate chambers, straw-tube detectors, and plastic scintillator hodoscopes. Presently, we already got start-up funds from the National Natural Science Foundation of China and RIKEN, and hopefully, Chinese Academy of Sciences will provide the funding gap for construction of the experimental setup.

We have estimated production yields of hypernuclides by using projectile fragmentations. Let us take 4.25 A GeV ^{20}Ne projectiles as an example to demonstrate the superiority for study of hypernuclides at HIAF. In bombardment on a massive diamond target with ^{20}Ne projectiles, a large variety of hypernuclides can be produced. Given that the intensity of ^{20}Ne beam is 10^7 particles per second, the production rates for many species of single- and double-strangeness hypernuclides are expected to be as high as 8×10^5 and 6×10^2 per day, respectively. Therefore, it provides us a great opportunity to explore the hitherto unknown territories in hypernuclide chart. We will identify new hypernuclides with the invariant mass method and determine their half-lives from the flight length distribution. With 1-day measurement, about one million single-Λ events are accumulated, and thus half-lives of Λ-hypernuclides can be determined to a precision of 0.5 ps. For double-strangeness hypernuclides, 4-week measurements can yield their half-lives with a precision around 10 ps. In addition, neutral hypernuclides such as ΛnnΛΛn, and ΛΛnn can be produced and studied very precisely. The setup can also be mounted at a mid-focal plane of HFRS. By using high-energy neutron-rich secondary beams, we can produce neutron-rich Λ-hypernuclides and even search for neutron-rich Σ-hypernuclides via charge-exchange reactions.

Plenty of hypernuclides are expected to be produced and identified at HIAF. Hopefully, the drip lines of Λ-hypernuclide chart can be reached for light hypernuclides, and many Σ-hypernuclides could be observed. With valuable high-precision and large data samples of binding energies and half-lives of hypernuclides, we can probe the fundamental baryonic interactions.

4.2.2 Phase diagram of strongly interacting matter

QCD theory describes the interactions between quarks and gluons and the properties of strongly interacting matter. In QCD, the net-baryon number B of a bulk matter is conserved, and hence, the corresponding chemical potential μ_B is defined, which denotes the energy variation in the system while changing one unit of the quantity B. Thermodynamically, a conventional temperature Tc is adopted as an intrinsic scale of bulk hadronic matter [30]. Tc is defined theoretically, and it is finite and changes

with μ_B [31]. Just like water, the Celsius scale of temperature is defined by the boiling point of water at normal pressure, and the boiling point changes with pressure. The phase diagram of strongly interacting matter can be depicted using μ_B and temperature T scaled by T_C [32]. Lattice QCD calculations predicted that a line of first-order phase transition separates the low-temperature hadronic gas phase from the high-temperature quark-gluon plasma [32]. This line begins at large μ_B and small T, curves gradually toward smaller μ_B and larger T, and eventually ends at the QCD critical point. Beyond the critical point, there are no phase transitions, the hadronic gas phase evolving smoothly into the quark-gluon plasma while increasing T. It is of utmost importance to study the phase diagram of strongly interacting matter and particularly to search for the critical point since they have a great impact on understanding of the strong interactions and the universe evolution at early stage [33, 34].

The critical point is a milestone in the QCD phase diagram and the Holy Grail in the field of heavy-ion collisions at relativistic energies [33, 34]. Searching for the critical point has triggered several experimental programs at facilities such as the Relativistic Heavy Ion Collider (RHIC), the Large Hadron Collider (LHC), the Super Proton Synchrotron (SPS), the Facility for Antiproton and Ion Research (FAIR), and the Nuclotron-based Ion Collider Facility (NICA). Recently, a beam energy scan measurement was carried out at RHIC, and intriguing non-monotonic behavior as a function of collision energy was observed in the net-proton fluctuation, likely indicating existence of the critical point [35]. This phenomenon occurs at the low-energy end at RHIC. HIAF can extend the coverage of μ_B to lower energy. The beam energy scan program would be incomplete without the results from the energy domain at HIAF.

We are building the external target experiment setup dedicated to study of the QCD phase structure and nuclear matter equation of state. This setup, as shown in Fig. 7, is composed of a superconducting dipole magnet, a time projection chamber (TPC) and an inner time-of-flight detector (iToF) placed inside the magnet, a multi-wire draft chamber array (MWDC) and an external time-of-flight detector (eToF) covering the forward angle region, as well as a zero-degree detector (ZDC) behind eToF. With wide opening in both rapidity and azimuthal angles, momenta of charged particles produced in high-energy heavy-ion collisions are measured. After extensive R&D on key detectors and the associated electronics, we come to the construction stage with financial supports from the National Natural Science Foundation of China and Chinese Academy of Sciences. After commissioning in 2024, we will use the external target experiment setup to take data with a 0.5 GeV/u ^{238}U beam provided by HIRFL and then move it to the high-energy experimental station and search for the critical point in the energy region at HIAF.

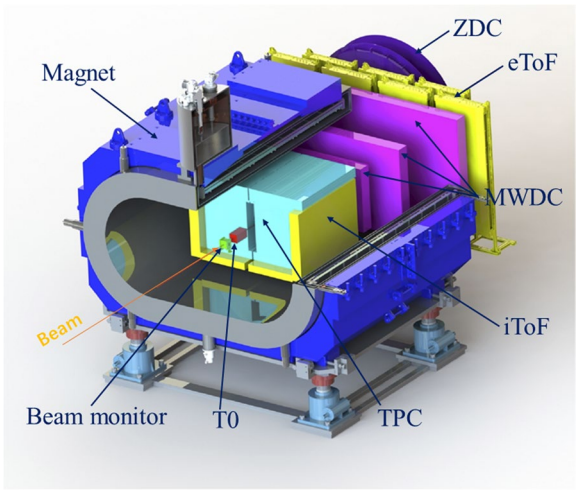

Fig. 7 The external target experiment setup with major components indicated

The primary goal is to search for the QCD critical point via beam energy scan measurements at HIAF. In addition, in relativistic energy heavy-ion collisions at HIAF, the peak nucleon density of produced nuclear matter can reach 2–3 times of the saturation density, which is an ideal sample for studying the symmetry energy essentially related to the equation of state of asymmetric nuclear matter at high density.

4.3 High-energy fragment separator

After discovery of the amazing neutron halo in ^{11}Li [36, 37], nuclear physics got through a Renaissance with the advent of radioactive isotope beam (RIB) facilities worldwide in late 1980s. Since then, the frontier of nuclear physics has been exploring the unknown territories in nuclide chart, where weakly bound nuclides with extreme neutron or proton excess are expected to have exotic structure and properties. Discoveries of new nuclear phenomena, such as neutron halo, evolution of magic numbers, soft excitation modes, and clustering structure, have steered development of nuclear theories from more basic foothold [33, 34]. Although the so-called state-of-the-art nuclear models have been developed, unified way of understanding of structure and properties in different regions in nuclide chart has remained as a great challenge. Meanwhile, nuclear reactions and decays occurring in stellar environments have been extensively studied using RIBs in laboratories, and the outputs have significantly deepened our understanding of various nucleosyntheses processes in explosive celestial environments and

production of chemical elements in the universe. However, the origin of heavy elements from iron to uranium has not yet been fundamentally resolved. The rapid-neutron capture process is proposed to produce about half of the elements beyond iron, which involves many extremely neutron-rich nuclides inaccessible at existing RIB facilities [33, 34].

Next-generation RIB line is a crucial facility to perform a large variety of modern nuclear physics experiments with outstanding potential for scientific discoveries [33, 34]. Based on the beam energies and intensities from the booster, we have surveyed the optimum experimental conditions for a batch of typical physics cases, such as the appropriate reactions to produce the exotic nuclides of interest and the required performance of RIB line including angular acceptance, momentum acceptance, and momentum resolution. Then, we have designed HFRS with a length of 192 m.

Primary beam bombards on a production target, and RIBs produced via projectile fragmentation or in-flight fission reactions are collected and purified by HFRS using the standard Bρ-ΔE-ToF method. Due to extremely strong radiations, the production target area is well shielded and closed, and robots perform all operations, for example, replacing the production target and beam monitoring equipment. HFRS can deal RIBs with a maximum magnetic rigidity of 25 Tm. This high rigidity enables HFRS to deliver high-energy neutron-rich rare isotope beams for experiments and opens the possibilities for some unique experiments like synthesis of neutron-rich hypernuclides and study of Δ-resonances in unstable nuclides, which have beam energy thresholds.

HFRS has a large acceptance. The angular acceptances are ± 30 mrad horizontally and ± 15 mrad vertically, and the momentum acceptance is ± 2%. These features allow us to collect reaction products with high efficiencies in both projectile fragmentations and in-flight fissions. Compared with the case of projectile fragmentations, fission fragments are produced with much larger angular and momentum spreads. For example, the standard momentum deviation and angular spread of ^{132}Sn fragments produced via 800 MeV/u ^{238}U fissions are about 3.5% and 15 mrad, respectively [38]. These distributions are comparable with the acceptances of HFRS, and an approximately 40% efficiency for collection of ^{132}Sn fragments in the energy domain can be attained.

Similar to other separators of the same generation in the world, such as SuperFRS and BigRIPS, HFRS has a two-stage configuration, and both stages are designed as point-to-point optical system. The first stage named pre-separator is 74 m in length and used to dump intense primary beams and undesired fragments after the target. The ion-optical layout of the pre-separator is presented in Fig. 8. Two sets of targets are optional at PF0 to produce RIBs, made from graphite and tantalum, respectively. The graphite target is used to produce RIBs via projectile fragmentations, and the tantalum one is for fission cases. An achromatic degrader (D1) is placed at the dispersive focal plane PF2 to purify the desired rare isotopes with subsequent dipole magnets. Unwanted reaction products are stopped by the slits at the focal planes PF2 and PF4. Unreacted projectiles are transmitted forward together with reaction products and must be removed efficiently with minimal influence on transmission of the products of interest. Therefore, the beam optics with strong focusing in x direction at PF1 is designed. The projectiles are intercepted in the beam dumps (BD1-BD6) installed after each dipole magnet according to Bρ difference between the projectiles and the ions of interest.

To meet the requirements for various experiments, two different ion-optical modes are designed for the second stage named the main separator. One is the dispersive mode in which the final focus is momentum dispersive, and the other is the achromatic mode with the final achromatic focus. Figure 9 shows schematically the layout of the main separator and the experimental setups for the two modes.

In the dispersive mode, the main separator is operated as a separator and spectrometer. The first part from MF0 to MF4 is used to separate and identify rare isotopes. A

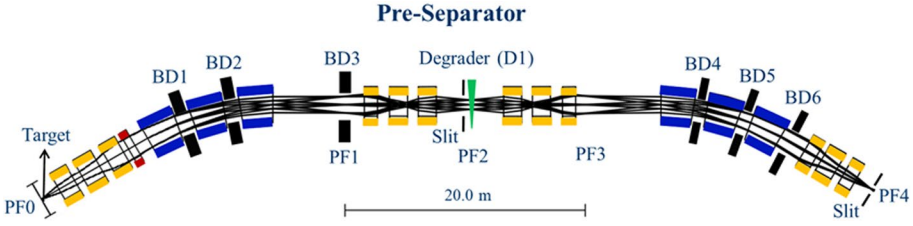

Fig. 8 Layout of the pre-separator. PF0-PF4 are the focal planes, and BD1-BD6 are the beam dumps. Ion trajectories with three divergence angles and three momentum deviations are schematically depicted in the first-order approximation. Dipole magnets are indicated in blue and quadrupole magnets in golden. The magnets are resistant to radiations

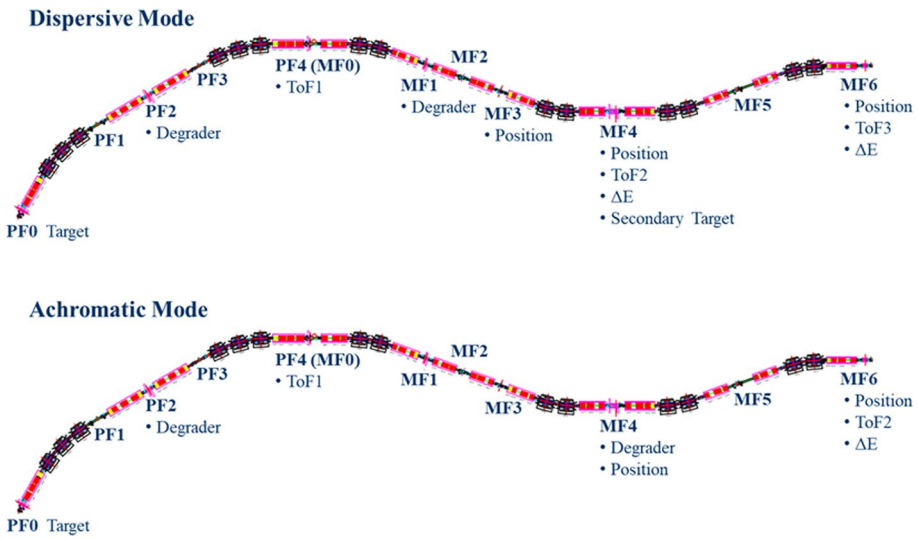

Fig. 9 Schematic views of the experimental setups for the dispersive mode (upper) and the achromatic mode (lower). The foci are indicated. The main separator from MF0 to MF6 comprises superconducting dipole magnets in black and multipole magnets in pink

second degrader at MF1 is employed to reduce the contaminants caused by secondary reactions and charge state change in the first degrader. A secondary reaction target at MF4 is used in this mode. Hydrogen and deuteron targets are under development. The second part from MF4 to MF6 works as a zero-degree spectrometer to study the secondary reaction products. This mode has two important dispersive planes of MF1 and MF6. The first order momentum resolution is 700 at MF1 and 1100 at MF6 for an emittance of 30 πmm·mrad and a horizontal beam spot size of ± 1 mm at MF0.

In the achromatic mode, the main separator is operated as a single separator with an achromatic degrader at MF4. It is a point-to-point focusing optical system with image magnification of one at the focal plane MF6 in both horizontal and vertical directions. There has one important dispersive plane at MF4, whose first-order momentum resolution is 1100 for an emittance of 30 πmm·mrad and a horizontal beam spot size of ± 1 mm at MF0. In this mode, RIBs can also be delivered further from MF6 to the external terminal, as shown in the upper right corner of Fig. 2, through a beam transfer line with a length of 52 m. In the external terminal, there is large space for experimental instruments. This beam line is a point-to-point focusing optical system and has the same acceptances and maximum magnetic rigidity as HFRS.

Plenty of exotic nuclides far from the β-stability line can be produced and delivered by HFRS for fixed target experiments. In these experiments, secondary cocktail beams are identified in the main separator with the ΔE-ToF-Bρ method, in which the energy lose (ΔE), the time-of-flight (ToF), and the magnetic rigidity ($B\rho$) are measured and used to determine the atomic number Z and A/Q ratio of the rare isotopes of interest. In the dispersive mode, ΔE detectors placed at MF4 and MF6 provide energy loss information, timing detectors located at MF0, MF4, and MF6 with a flight path of 65 m and 53 m provide ToF information, and $B\rho$ values are determined from position measurements at MF3, MF4, and MF6. Using the data measured, we can make clear particle identification before and after the secondary reaction target at MF4, respectively. In the achromatic mode, ΔE is obtained by detector at MF6, ToF value is measured by detectors at MF0 and MF6 with a long flight path of 118 m, and $B\rho$ value is determined by position detectors at MF4 and MF6.

The features of HFRS make it possible to produce intense RIBs. The unprecedented RIB intensities require development of high resolving power and high-rate detectors for particle identification. From simulations of particle identification in typical reactions, it requires that the detectors should have performances of 40 ps time resolution, 1.0 mm position resolution, or 0.5% energy resolution. Multiple sampling ionization chambers are under construction as energy loss detectors, which are extremely stable under beam bombardments and have energy resolution as good as that of semiconductor detectors. The superior radiation resistance and excellent time performance have made diamond detectors first choice for ToF measurements. For the position measurement, GEM-TPC detectors are

employed owing to their excellent performance under condition of intense beams.

HFRS is designed as a world-unique facility, and its peculiarities are as follows:

HFRS has the maximum magnetic rigidity of 25 Tm, and thus, it can produce high-energy RIBs with energy up to 2.9 GeV/u for $A/Z=2$ nuclides and 1.7 GeV/u for $A/Z=3$ nuclides.

HFRS has high primary beam suppression power and excellent separation power of radioactive nuclides up to uranium.

HFRS can provide fully stripped radioactive ions of all elements from hydrogen through uranium.

HFRS is a versatile spectrometer with either dispersive mode or achromatic mode using different ion-optical settings.

The research program based on HFRS emerges from experiments performed at existing RIB facilities around the world [33, 34]. It will exploit HFRS as a flexible, high-resolution ion-optical device. A white paper, entitled as physics at HIAF high-energy fragment separator, is ready and will be released soon. In this document, we outline new opportunities for nuclear physics and nuclear astrophysics at relativistic energies that can be addressed at HFRS. We focus on new isotope searching, fundamental properties of exotic nuclides, correlations in finite nuclides, evolution of nuclear shell structure far away from the β-stability line, dynamical symmetries in exotic nuclides particularly along the $N=$ Z line, and researches of astrophysical relevance.

Last but not least, HFRS features with the highest magnetic rigidity — up to 25 Tm — as compared with any existing or planned RIB facilities. It reinforces HFRS with a large discovery potential, and unique experiments are in consideration, including nucleon excitations inside unstable nuclides, new giant resonance of neutron-rich nuclides, spectroscopy of exotic meson-nucleus bound system, and synthesis of neutron-rich hypernuclides [39]. Here, let us take the Δ-resonances in nuclear medium as an example to demonstrate the uniqueness of HFRS. In charge-exchange reactions at relativistic energies, nucleon inside a nuclide can be excited, providing a unique way to study Δ-resonances in nuclear medium. The Δ-resonance is a spin- and isospin-flip intrinsic excitation of a nucleon, and its fundamentality is that the amazing three-body force in nuclides is proposed to originate from Δ-resonances. Hitherto, Δ-resonances have been studied exclusively in stable or near stable nuclides [39]. HFRS enables us to study Δ-resonances in nuclear medium over long isotopic chains from the stability to approaching the drip lines. The systematic investigation can shed light on the questions of crucial importance: are the masses and lifetimes of Δ-resonances modified in nuclear medium? How deep is the Δ-nuclide potential? What is the isospin dependence of the resonance potentials? For these experiments, dedicated experimental setups will be built and coupled to specific focal planes of HFRS.

4.4 Spectrometer ring

In a fast beam extraction mode of the booster, HFRS works either as a beam line delivering highly charged ions into the spectrometer ring or as a separator without clear identification for single ion. In the latter case, all the reaction products with same $B\rho$ are transferred into the spectrometer ring for further identification and experimental study. The spectrometer ring is in essence a storage ring equipped with an electron cooler and a stochastic cooling device. Based on the spectrometer ring, we will build a dielectronic recombination spectrometer, an isochronous mass spectrometer, and a setup for in-ring nuclear reactions. With these setups, we mainly measure nuclear masses, reaction cross sections, and exotic decay modes and resonant excitations of highly-charged ions. Of high-priority research program is to measure systematically nuclear masses in broad regions.

4.4.1 Setups for atomic physics with relativistic heavy ions

Atomic physics with highly charged ions at storage rings has been developed for over two decades, which opens new research areas in structure and reaction mechanism of highly charged ions as well as experiments at the interface of atomic physics and nuclear physics. The researches aim at studying preciously quantum electrodynamics (QED) effects and electron correlations in strong Coulomb fields, understanding ultrafast collision dynamics at relativistic energies, and recognizing exotic properties of radioactive ions. The spectrometer ring provides a wonderful platform for atomic physics with relativistic highly charged ions.

The electron cooler at the spectrometer ring can produce cold electron beam with a longitudinal temperature of less than 1.0 meV. Interacting with the cooling electrons results in a very narrow momentum spread of ions stored, down to the order of 10^{-5} achievable. Based on a dedicated electron target, high-resolution spectroscopic studies of highly charged ions will be conducted. The transverse and longitudinal electron temperatures in the electron target are significantly reduced by the adiabatic magnetic expansion and the adiabatic acceleration, respectively. In a straight section of the electron target, ion beam is merged with ultracold electron beam. If an initial ion with charge state A^{q+} captures a free electron

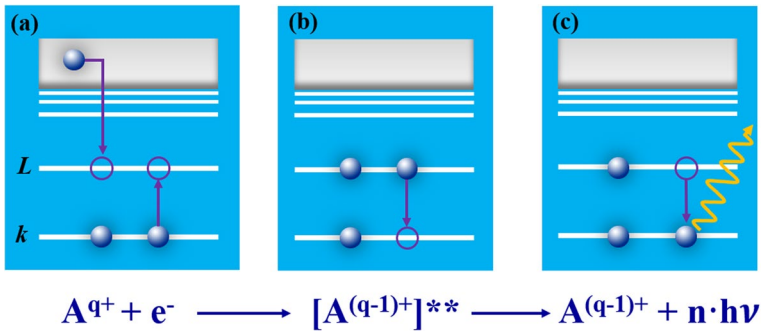

Fig. 10 Schematic diagram of the KLL-DR process of a He-like ion. KLL-DR process means that a free electron is captured into the L orbit of the ion, and simultaneously, a bound electron is excited from the K orbit to L orbit

with well-defined kinetic energy provided by the electron target and a bound electron is resonantly excited simultaneously, the so-called dielectronic recombination (DR) process occurs. DR is a fundamental electron–ion collision process. As shown in Fig. 10, DR is a two-step resonant process, and the doubly excited state decays via radiative process.

By detuning precisely and step wisely the electron energy from the cooling point, the resonances are measured by recording the number of recombined ions $A^{(q-1)+}$ as a function of the electron energy. From detailed analysis of DR spectra, precise transition energies of core electrons are obtained. Then, we can derive valuable information on the Lamb shift of energy levels, the electron correlations such as Breit interaction, the nuclear charge radius, the hyperfine structure, and the hyperfine-induced transition rate of the stored ions [40–42]. This type of DR spectrometry has been well established at the storage rings at GSI and IMP [43–46], which is applicable to not only stable ions but also unstable ions and nuclear isomers.

Based on the electron cooler and the ultracold electron target, we have designed the dielectronic recombination spectrometer [47, 48], as shown in Fig. 11. The recombined ions are separated from the stored beam in the downstream dipole magnets and then detected by the particle detectors installed at the outer side of the ring. The electron target and the detector system are under construction. This spectrometer will provide excellent opportunities for precision DR spectroscopy of H- and He-like heavy ions. In addition, other experiments with highly charged ions are planned, including collision dynamics of relativistic highly charge ions with atoms, molecules, or clusters in zepto-second time

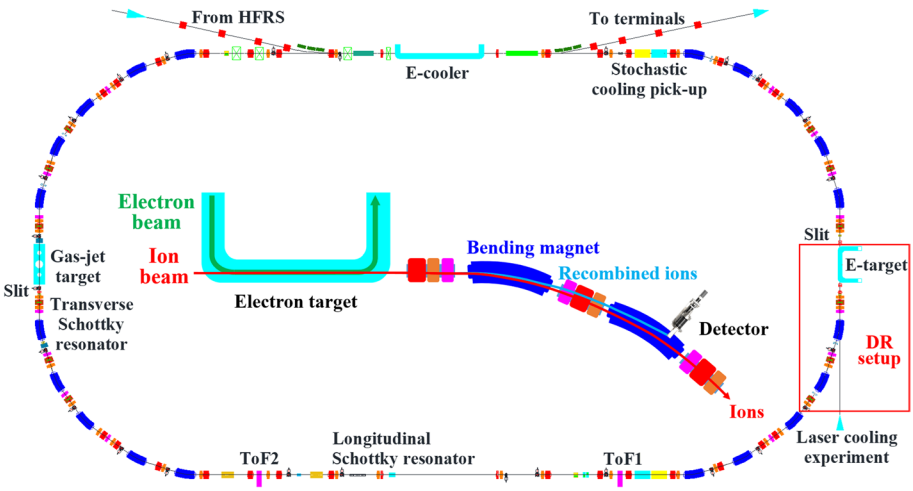

Fig. 11 A sketch of the dielectronic recombination spectrometer at the spectrometer ring. The DR experimental region is indicated with the red box, which is enlarged and inserted in the middle of the figure. The components of a stochastic cooling device are indicated, including the stochastic cooling kicker, the longitudinal Schottky resonator, and the transverse Schottky resonator. E-cooler and E-target stand for the electron cooler and electron target, respectively. The isochronous mass spectrometer is built using the time-of-flight detectors ToF1 and ToF2, and the setup for in-ring nuclear reactions is built at the gas-jet target

scale employing a reaction microscope, X-ray spectroscopy of highly charged ions at an internal gas target, and laser cooling and laser spectroscopy of relativistic heavy ions [47, 48]. The design of experimental setups is being undertaken.

Bound electrons of high-energy ^{238}U ions extracted from the booster can be fully stripped with a charge stripper at the primary target position of HFRS. Bare ^{238}U ion beam brings about opportunities for novel experiments. Here, we briefly introduce a unique experiment based on double storage rings. It was predicted theoretically in 1970s that the vacuum becomes unstable and decays via spontaneous electron−positron pair creation if the electromagnetic field is stronger than the Schwinger limit (1.3×10^{16} V/cm) called the super-critical field [49]. Search for the electron−positron pair creation in super-critical field is a long-term pursuit goal of QED. In practice, the only way acquiring such strong field is to produce instantly a composite nuclear system with charge number larger than 173. For this purpose, slow collisions involving highly charged ions at a center-of-mass energy below the Coulomb barrier were proposed [50, 51]. Compared with the experiments by colliding highly charged heavy ions with solid high-Z target, the fields created by the collisions of bare ions are much stronger, and the Pauli blocking effect caused by filled electrons is avoided, resulting in the pair production cross section enhanced for more than two orders of magnitude [50, 51]. Moreover, collision of bare ions in high vacuum environment is electron background-free, which improves experimental sensitivity and reliability. At HIAF, unique experiment using merged ^{238}U beams with the spectrometer ring and another merging ring is proposed. The two rings store bare ^{238}U ions with well-defined energies. The principal goal is to study the super-critical field effect. The idea is to merge two bare ^{238}U ion beams stored in the rings in a colliding zone with a beam crossing angle of about 6°, to generate the super-critical field at the instant when two ^{238}U ions approach sufficiently close to each other and form a two-center nuclear system, and to detect coincident electron and positron emitted from the collisions at low center-of-mass energies. In addition, H-, He-, or Li-like heavy ions are optional as the merged beams, and we can study the QED effects in extremely strong fields by measuring X rays from quasi-molecules at low collision energies [52]. The merging ring and colliding section as well as the detector system are under design presently.

4.4.2 A novel isochronous mass spectrometer

The mass represents a basic nature of nuclides. The difference between the mass of a nuclide and the sum of the masses of its constituent-free nucleons, i.e., the binding energy, provides direct information about the complex interactions that are responsible for nuclear binding. Accurate and precise masses of atomic nuclides are crucial in studies of a variety of phenomena in nuclear structure and nuclear astrophysics, as well as for testing fundamental interactions and symmetries [53–56]. Masses of about 2550 nuclides are known experimentally to date [57], and potentially over 4000 nuclides are yet to be discovered and measured [58]. Of present interest are the masses of nuclides lying far away from the valley of the β-stability line [59]. Especially, masses of extremely neutron-rich nuclides are needed for modelling the rapid-neutron capture nucleosynthesis [60]. Such nuclides are inevitably short-lived and have tiny production yields, making their mass measurements extremely challenging. Therefore, it is strongly demanded to develop measurement techniques capable of determining precisely the mass of a single, short-lived particle.

Isochronous mass spectrometry (IMS) at heavy-ion storage rings is suited for mass measurements of exotic nuclides with short lifetimes down to several tens of microseconds [61, 62]. Since the pioneering experiments conducted at ESR at GSI, Germany [61, 62], IMS has been established at the experimental cooler storage ring (CSRe) at IMP [63], China, and at the Rare-RI Ring at RIKEN, Japan [64]. In conventional IMS, the isochronous condition is fulfilled only for the ion species in a limited range of mass-to-charge (m/q) ratios, while the resolving powers are inevitably deteriorated for other ion species outside the narrow isochronous window. In addition, the momentum distributions of different ions injected into a ring are not the same, generally asymmetric and inhomogeneous due to mechanisms of production reactions. This would lead to systematic deviation in the mass determination.

In order to improve the mass resolving power of conventional IMS as well as to eliminate systematic deviation in a broad m/q range, a preliminary idea was conceived to measure the velocity of each stored ion [65–67]. We have extensively studied this conceptual idea theoretically and technically [68]. Given that the revolution time T and velocity v of individual ion are measured with high accuracy and precision [69], we have successfully established a novel mass spectrometry, named as the $B\rho$-defined IMS. The principle is described briefly as follows. Two identical ToF detectors are placed in a long straight section of a storage ring. Each detector consists of a thin carbon foil (ϕ40 mm, 18 μg/cm^2) and a set of microchannel plates (MCP) [70]. When an ion passes through the carbon foil, secondary electrons are released from the foil surface and isochronously guided to the MCP by perpendicularly arranged electric and magnetic fields. Fast timing signals from the two MCPs are recorded by a digital oscilloscope at a sampling rate of 50 GHz. The

time resolution of the ToF detectors is determined to be around 20 ps using ^{241}Am α source. With the T and v values determined through the procedure described in [69], the magnetic rigidity $B\rho$ and orbit length C of the stored ion are obtained via the following:

$$\mathrm{B}\rho = \frac{\mathrm{m}}{\mathrm{q}}\gamma\upsilon \tag{1}$$

and

$$\mathrm{C} = \mathrm{T}\upsilon \tag{2}$$

where the Lorentz factor $\gamma = {}^{1}\!\Big/\!{\sqrt{1-\beta^2}}$ with β being the velocity in unit of the speed of light in vacuum. $B\rho$ and C are correlated and exhibited as a curve in the Bρ-C plane, which characterizes the movement of all ions in the ring. The experimental $\left\{\mathrm{B}\rho^{\mathrm{i}}_{\mathrm{exp}}, \mathrm{C}^{\mathrm{i}}_{\mathrm{exp}}, \mathrm{i} = 1, 2, 3, \ldots\right\}$ data are obtained with the equations. Using well-known masses with high accuracy, the Bρ(C) function can be constructed by a least-square fit to the $\mathrm{B}\rho_{\mathrm{exp}} \sim \mathrm{C}_{\mathrm{exp}}$ data. Therefore, the m/q values of any stored ions including the unknown-mass nuclides are derived directly according to the following:

$$\left(\frac{\mathrm{m}}{\mathrm{q}}\right)^{\mathrm{i}}_{\mathrm{exp}} = \frac{\mathrm{B}\rho\left(\mathrm{C}^{\mathrm{i}}_{\mathrm{exp}}\right)}{(\gamma\upsilon)^{\mathrm{i}}_{\mathrm{exp}}}. \tag{3}$$

This equation is the basic formula of the $B\rho$-defined IMS, and the Bρ(C) function is a universal calibration to be used for mass determination. Details of this novel IMS will be presented in a forthcoming paper.

The feasibility of the novel IMS has been proved by measuring masses of neutron-deficient fp-shell nuclides at CSRe, which were produced by fragmenting the 440 MeV/u ^{58}Ni projectiles on a ^{9}Be target. The well-known masses of $T_Z = -1/2$ nuclides were employed for calibrations, and the masses of $T_Z = -1$ nuclides were determined with the conventional IMS and $B\rho$-defined IMS. Each of the calibrants was also supposed, one by one, to be unknown, and its mass was redetermined using the remaining reference nuclides as calibrants. The normalized $\chi_{\mathrm{n}} = 0.98$ and 0.78 for the masses determined presently indicate that the quoted uncertainties are conservative. Figure 12 compares the masses to the tabulated ones [57]. Large systematic deviations with the conventional IMS are observed. Such deviations can be reduced by restricting the $B\rho$ acceptance of a ring but at a cost of dramatically reduced efficiency. In contrast, by using the $B\rho$-defined IMS, not only are the systematic deviations removed but also the mass precisions are improved significantly over a broad m/q range. The $B\rho$-defined IMS has the following outstanding merits:

Ultimate sensitivity: Every ion stored in a ring is unambiguously identified, and revolution time and velocity of each individual ion are measured.
Rapid measurement: The overall measurement duration is as short as 400 μs, and therefore, the method is applicable to all nuclides lying within drip lines.
High precision: Precision as good as a few keV is achievable for nuclides with tiny production yields, and in a limiting case of just a single ion with a charge state of q, its mass can be determined with a precision of ~ 5·q keV.

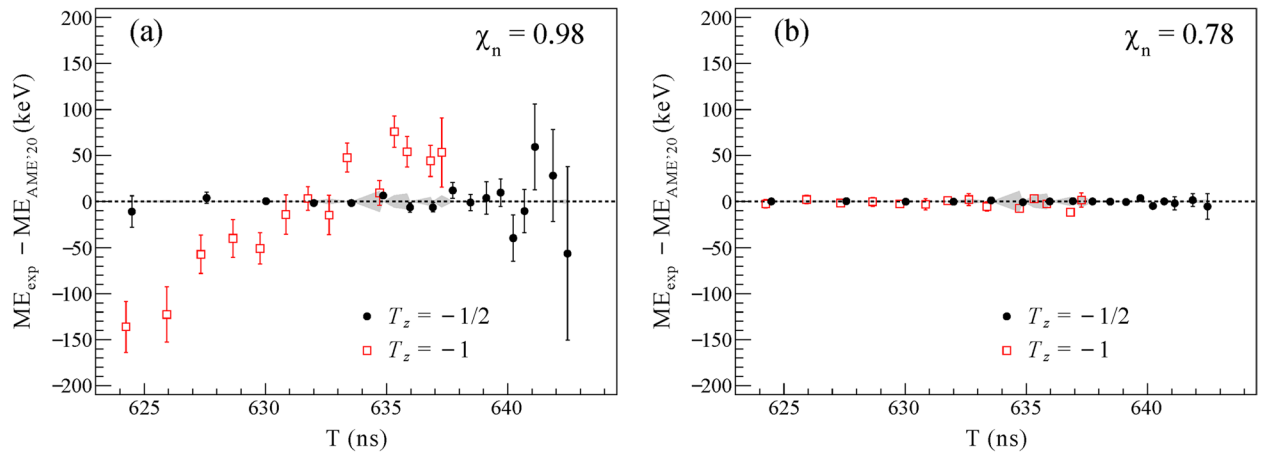

Fig. 12 Mass excesses (ME) of $T_Z = -1$ nuclides (red open squares) and $T_Z = -1/2$ nuclides (black dots), represented with respect to the values in AME2020 [57]. Left, results obtained with the conventional IMS. Right, results with the $B\rho$-defined IMS. The gray shadow shows the uncertainties in AME2020 [57]

Broadband measurement: Masses of nuclides within a broad range of m/q can be measured simultaneously in one experimental setting.

In short, the *B*ρ-defined IMS boosts significantly the efficiency, accuracy, and precision of mass measurements. It is really a major breakthrough of the storage-ring-based mass spectrometry. This novel IMS has been established at CSRe in Lanzhou and will be certainly adopted at a long straight section of the spectrometer ring by using the two ToF detectors as shown in Fig. 11.

We plan to measure systematically masses of nuclides in their ground or isomeric states. With accurate and precise mass data, we will probe some of the most fundamental questions in nuclear physics, such as exotic decay modes of drip-line nuclides, breaking of isospin symmetry and nucleon paring along $N=Z$ line, disappearance of spherical magic numbers and appearance of new magic numbers, and onset of deformation along isotopic chain [33, 34]. The development of nuclear models crucially depends on nuclear masses as experimental input, and such data are particularly valuable if obtained for long chains of isotopes or isotones. Systematic new masses will be used to constrain and develop nuclear models. In addition, precision nuclear masses are of utmost importance to simulate various nuclear processes in staller environments. Taking the nuclear masses as inputs of modelling the rapid-neutron capture process, we anticipate to have an insight into the origin of heavy elements in the universe and the dynamics of the explosive core-collapse supernovae and two neutron star mergers.

4.4.3 Setup for in-ring nuclear reactions

Proton elastic scattering off nuclide has been used generally for measuring nuclear matter distributions and deducing optical model potentials (OMPs) [71, 72], which are essential for the description of direct reactions involving exotic nuclides with the distorted-wave Born approximation. With scattering data on stable nuclides, the global phenomenological parameters of OMPs in the energy region up to 200 MeV are determined theoretically. However, it is proven that the radial shape and strength of the OMPs depend strongly on the proton-neutron asymmetry [72], and therefore, the OMPs deduced from stable nuclides cannot be applied directly to describing the scattering process of unstable nuclides. Proton elastic scattering was performed extensively in direct kinematics, i.e., proton beams interact with a target made of the nuclides of interest [71]. Obviously, such kind of experiments is limited to stable or very long-lived nuclides. In order to study proton scattering off unstable nuclides, experimental method of inverse kinematic employing hydrogen target has been established at RIB facilities. Based on storage rings, novel experimental approaches, in which stored ions interact with internal gas-jet target, have been developed to measure nuclear matter distributions, giant resonant strengths, and astrophysical reaction rates [73–75]. The experiments of in-ring nuclear reactions benefit from the extremely low background in high vacuum, the high luminosity repeatedly using ions stored, and the high-resolution measurement inherent to negligible straggling of the scattered projectiles in a thin gas target.

The critical point for in-ring reaction experiments is to develop position-sensitive silicon strip detectors applicable to ultrahigh vacuum environment. We have designed and fabricated single-sided silicon detectors with a thickness of 300 μm and an active area of 48×48 mm^2. The detectors have good energy resolution and particularly are fully compatible with ultrahigh vacuum [76]. At CSRe, we performed an experiment of 95 MeV/u stored $^{58}Ni^{19+}$ ions interacting repeatedly with an internal hydrogen gas target and measured low-energy recoiling protons from the elastic collisions by using the detector newly developed [77]. This successful experiment has paved the way for studies of nuclear reactions at the spectrometer ring. The setup for in-ring nuclear reactions with a gas jet target is designed and now under construction [2].

With the setup for in-ring nuclear reactions, the primary physical goal is to measure the differential cross sections of proton elastic scattering off unstable nuclides at low momentum transfer and then determine the size and radial shape of nuclear matter distributions in exotic nuclides. Combining the proton-distribution radii determined by other methods, we can study the change of neutron skin thicknesses along isotopic chains. The systematic neutron skin thicknesses can be used to stringently constrain the equation of state of asymmetric nuclear matter, which is crucial to understand the properties of exotic nuclides and compact neutron stars. The nuclear density near the maximum of $r^2\rho(r)$ is sensitive to the saturation density of nuclear matter, and therefore, the isospin dependence of the saturation density can be studied from the systematic change of the nuclear density in a broad range of nuclides from the β-stability line to very neutron-rich nuclides [39]. In addition, experiments of direct reactions induced by proton or other light particles in inverse kinematics will be carried out in order to measure the reaction rates of astrophysical relevance, for instances, the (p, γ), (α, p), (α, n), and (α, γ) reaction rates, which are indispensable inputs of modelling nucleosynthesis processes in stellar environments [33, 34].

5 Summary and outlook

HIAF is a next-generation research facility for heavy-ion science and technology, complementary to the same kind of facilities in the world. The facility construction is on time schedule and will be into operation at the beginning in the year of 2026. HIAF features with unprecedented beam intensities and broad beam energies from MeV/u to GeV/u, and a large variety of exotic nuclear matters can be produced. Based on HIAF, we aim at establishing a heavy-ion science and technology research center. Researchers from all over the world explore the hitherto unknown territories in nuclide chart, approach the experimental limits, open new domains of physics researches in experiments, and develop new heavy-ion applications. During the construction phase, we make much account of future upgrades of HIAF. The linear accelerator is planned to be extended, and $^{238}U^{35+}$ beam can be accelerated to 150 MeV/u energy. The tunnel for extension of the accelerator and the associated experimental hall are already built. The China ADS facility is under construction on the same campus of HIAF, and its driver is a powerful proton Linac with a designed power of 1.5 GeV@10 mA. HIAF can incorporate with an ISOL source driven by the proton Linac, and consequently, HIAF can turn into the first "full featured" facility in the world, which is capable of producing RIBs using target spallation, projectile fragmentation, in-flight fission, and even hybrid method. The end of the Linac is laid close to the ion source of HIAF, and the area housing an ISOL source is kept. HIAF must be a domestic user facility and should be an international user facility. We welcome interested users to participate the design and construction of experimental setups and conduct researches at HIAF.

Acknowledgements
The authors thank XM, LTS, LNS, and YPZ for fruitful discussions and/or critical reading of the manuscript.

Authors' contributions
ZXH is the deputy director of HIAF project and coordinates the design and construction of experimental setups of HIAF. YJC is the chief engineer of HIAF project and coordinates the design of accelerator complex of HIAF. ZXH and YJC wrote and revised the manuscript. The authors read and approved the final manuscript.

Authors' information
Xiaohong Zhou is a Senior Researcher and the Head of the Center of Nuclear Physics at the Institute of Modern Physics, Chinese Academy of Sciences.</SimplePara><SimplePara>Jiancheng Yang is a Senior Researcher and the Head of the Center of Accelerator Physics at the Institute of Modern Physics, Chinese Academy of Sciences.

Funding
Xiaohong Zhou is financially supported by the National Natural Science Foundation of China Grant No. 11735017 and No. 12121005.

Availability of data and materials
All data and figures presented in this article are based on the materials available in public through the corresponding references with their permissions.

Declarations

Ethics approval and consent to participate
Not applicable.

Consent for publication
Not applicable.

Competing interests
The authors declare that they have no competing interests.

Received: 6 September 2022 Accepted: 21 October 2022
Published online: 08 November 2022

References

1. J.C. Yang, J.W. Xia, G.Q. Xiao et al., High intensity heavy ion accelerator facility (HIAF) in China. Nucl. Instrum. Meth. A. **317**, 263–265 (2013)
2. X.H. Zhou, Construction of the high intensity heavy-ion accelerator facility (HIAF). AAPPS Bull. **29**(2), 6–12 (2019)
3. Q. Wu, H.Y. Ma, Y. Yang et al., Status of intense permanent magnet proton source for China-accelerator driven subcritical system Linac. Rev. Sci. Instrum. **87**, 02B903 (2016)
4. L. Sun, J.W. Guo, W. Lu et al., Advancement of highly-charged ion beam production by superconducting ECR ion source SECRAL. Rev. Sci. Instrum. **87**, 02A707 (2016)
5. L. Sun, H.W. Zhao, J.W. Guo et al., *Challenges for the next-generation ECRIS. Proceedings of HIAT 2015* (JACoW Publishing, Yokohama, 2015), pp.268–270
6. L. Sun, W. Lu, H.W. Zhao et al., Progress on the development of key technologies for the fourth generation ECR ion source FECR. J. Phys. Conf. Ser. **2244**, 012021 (2022)
7. C. Wang, W. Dou, Z. Wang et al., Beam dynamics design of HIAF RFQ. Inter. J. Mod. Phys. E **30**(12), 2150104 (2021)
8. C.R. Prior, G.H. Rees, Multiturn injection and lattice design for HIDIF. Nucl. Instrum. Meth. A. **415**, 357–362 (1998)
9. N. Bohr, J.A. Wheeler, The mechanism of nuclear fission. Phys. Rev. **56**, 426–450 (1939)
10. M. Brack, J. Damgaard, A.S. Jensen et al., Funny Hills: the shell-correction approach to nuclear shell effects and its applications to the fission process. Rev. Mod. Phys. **44**, 320–405 (1972)
11. V.M. Strutinsky, Shell effects in nuclear masses and deformation energies. Nucl. Phys. A **95**, 420–442 (1967)
12. S.G. Nilsson, C.F. Tsang, A. Sobiczewski et al., On the nuclear structure and stability of heavy and super-heavy elements. Nucl. Phys. A **131**, 1–66 (1969)
13. Yu.T. Oganessian, A. Sobiczewski, G.M. Ter-Akopian, Super-heavy nuclei: from predictions to discovery. Phys. Scr. **92**, 023003 (2017)
14. Yu.T. Oganessian, V.K. Utyonkov, Super-heavy element research. Rep. Prog. Phys. **78**, 036301 (2015)
15. S. Hofmann, G. Munzenberg, The discovery of the heaviest elements. Rev. Mod. Phys. **72**(3), 733–767 (2000)
16. K. Morita, SHE research at RIKEN/GARIS. Nucl. Phys. A **944**, 30–61 (2015)
17. V.I. Zagrebaev, W. Greiner, Cross sections for the production of superheavy nuclei. Nucl. Phys. A **944**, 257–307 (2015)
18. A. Turler, R. Eichler, A. Yakushev, Chemical studies of elements with $Z \geq 104$ in gas phase. Nucl. Phys. A **944**, 640–689 (2015)
19. A. Ghiorso, S. Yashita, M.E. Leino et al., Sassy, a gas-filled magnetic separator for the study of fusion reaction products. Nucl. Instrum. Meth. A. **269**(1), 192–201 (1988)
20. M. Leino, Gas-filled separators-an overview. Nucl. Instrum. Meth. A. **204**, 129–137 (2003)
21. Z.Y. Zhang, L. Ma, Z.G. Gan et al., A gas-filled recoil separator. SHANS. Nucl. Instrum. Meth. B. **317**, 315–318 (2013)

22. L.N. Sheng, Q. Hu, H. Jia et al., Ion-optical design and multiparticle tracking in 3D magnetic field of the gas-filled recoil separator SHANS2 at CAFE2. Nucl. Instrum. Meth. A. **1004**, 165348 (2021)
23. V.I. Zagrebaev, W. Greiner, Production of heavy trans-target nuclei in multi-nucleon transfer reactions. Phys. Rev. C **87**, 034608 (2013)
24. J.V. Kratz, W. Loveland, K.J. Moody, Syntheses of transuranium isotopes with atomic numbers $Z \leq 103$ in multi-nucleon transfer reactions. Nucl. Phys. A **944**, 117–157 (2015)
25. Z. Xiaohong, Z. Zhiyuan, G. Zaiguo et al., Research program of super-heavy elements and nuclides based on HIAF. SCIENTIA SINICA Physica, Mechanica & Astronomica **50**(11), 112002 (2020)
26. M. Danysz, J. Pniewski, Delayed disintegration of a heavy nuclear fragment. Phil. Mag. **44**, 348–350 (1953)
27. D.H. Davis, 50 years of hypernuclear physics: I. The early experiments. Nucl. Phys. A **754**, 3–13 (2005)
28. O. Hashimoto, H. Tamura, Spectroscopy of Λ hypernuclides. Prog. Part. Nucl. Phys. **57**, 564–653 (2006)
29. T.R. Saito, W. Dou, V. Drozd et al., New directions in hypernuclear physics. Nat. Rev. Phys. **31**, 803–813 (2021)
30. Y. Aoki, Z. Fodor, S.D. Katz et al., The QCD transition temperature: results with physical masses in the continuum limit. Phys. Lett. B **643**, 46–54 (2006)
31. R. Brown, N.H. Christ, Y.F. Deng et al., Nature of the deconfining phase transition in SU(3) lattice gauge theory. Phys. Rev. Lett. **61**, 2058–2061 (1988)
32. S. Gupta, X.F. Luo, B. Mohanty et al., Scale for the phase diagram of quantum chromodynamics. Science **332**, 1525–1528 (2011)
33. NuPECC Long Range Plan 2017: perspectives for nuclear physics, available on the web at http://www.nupecc.org
34. Reaching for the horizon: the long rang plan for nuclear science, available on the web at https://science.energy.gov/np/nsac
35. Xu. Nu, K. Fukushima, B. Mohanty, The Little-Bang and the femto-nova in nucleus-nucleus collisions. AAPPS Bull. **31**, 1–16 (2021)
36. I. Tanihata, H. Hamagaki, O. Hashimoto et al., Measurements of interaction cross sections and nuclear radii in the light p-shell region. Phys. Rev. Lett. **55**, 2676–2679 (1985)
37. P.G. Hansen, B. Jonson, The neutron halo of extremely neutron-rich nuclei. Europhys. Lett. **4**(4), 409–414 (1987)
38. H. Geissel, H. Weick, M. Winkler et al., The Super-FRS project at GSI. Nucl. Instrum. Meth. B. **204**, 71–85 (2003)
39. Scientific Program of the Super-FRS Collaboration: report of the collaboration to the FAIR management, available on the web at https://www.gsi.de/en/researchaccelerators/fair.htm
40. C. Brandau, C. Kozhuharov, Z. Harman et al., Isotope shift in the dielectronic recombination of three-electron ANd^{57+}. Phys. Rev. Lett. **100**, 073201 (2008)
41. M. Lestinsky, E. Lindroth, D.A. Orlov et al., Screened radiative corrections from hyperfine-split dielectronic resonances in lithiumlike scandium. Phys. Rev. Lett. **100**, 033001 (2008)
42. S. Schippers, E.W. Schmidt, D. Bernhardt et al., Storage-ring measurement of the hyperfine induced $^{47}Ti^{8+}$ ($2s2p\ ^3P_0 \rightarrow 2s^2\ ^1S_0$) transition rate. Phys. Rev. Lett. **98**, 033001 (2007)
43. C. Brandau, C. Kozhuharov, Storage-ring studies of dielectronic recombination as a tool for precision spectroscopy, in *V. Atomic Processes in Basic and Applied Physics*. (Springer, Berlin, 2012), pp.283–306
44. M. Lestinsky, V. Andrianov, B. Aurand et al., Physics book: CRYRING@ESR. Eur. Phys. J. Special Topics **225**, 797–882 (2016)
45. Z.K. Huang, W.Q. Wen, X. Xu et al., Dielectronic and trielectronic recombination rate coefficients of Be-like Ar^{14+}. Astrophys. J. Suppl. Ser. **235**, 2 (2018)
46. Z.K. Huang, W.Q. Wen, S.X. Wang et al., Absolute rate coefficients for dielectronic recombination of Na-like Kr^{25+}. Phys. Rev. A **102**, 062823 (2020)
47. Z.K. Huang, W.Q. Wen, X. Xu et al., Dielectronic recombination experiments at the storage rings: from the present CSR to the future HIAF. Nucl. Instrum. Meth. B. **408**, 135–139 (2017)
48. X. Ma, W.Q. Wen, S.F. Zhang et al., HIAF: new opportunities for atomic physics with highly-charged heavy ions. Nucl. Instrum. Meth. B. **408**, 169–173 (2017)
49. B. Muller, J. Rafelski, W. Greiner, Electron shells in over-critical external fields. Z. Phy. A **257**, 62–77 (1972)
50. U. Muller, T. de Reus, J. Reinhardt et al., Positron production in crossed beams of bare uranium nuclei. Phys. Rev. A **37**, 1449–1455 (1988)
51. I.A. Maltsev, V.M. Shabaev, I.I. Tupitsyn et al., Electron-positron pair creation in low-energy collisions of heavy bare nuclei. Phys. Rev. A **91**, 032708 (2015)
52. A. Gumberidze, F. Bosch, A. Brauning-Demian et al., Atomic physics with highly-charged heavy ions at the GSI future facility: the scientific program of the SPARC collaboration. Nucl. Instrum. Meth. B. **233**, 28–30 (2005)
53. D. Lunney, J.M. Pearson, C. Thibault, Recent trends in the determination of nuclear masses. Rev. Mod. Phys. **75**, 1021–1082 (2003)
54. K. Blaum, High-accuracy mass spectrometry with stored ions. Phys. Rep. **425**, 1–78 (2006)
55. T. Eronen, A. Kankainen, J. Aysto, Ion traps in nuclear physics-recent results and achievements. Prog. Part. Nucl. Phys. **91**, 259–293 (2016)
56. J. Dilling, K. Blaum, M. Brodeur et al., Penning-trap mass measurements in atomic and nuclear physics. Ann. Rev. Nucl. Part. Sci. **68**, 45–74 (2018)
57. W. Huang, M. Wang, F. Kondev et al., The AME 2020 atomic mass evaluation (I). Evaluation of input data, and adjustment procedures. Chin. Phys. C **45**, 030002 (2021)
58. J. Erler, N. Birge, M. Kortelainen et al., The limits of the nuclear landscape. Nature **486**, 509–512 (2012)
59. T. Yamaguchi, H. Koura, Y. Litvinov et al., Masses of exotic nuclei. Prog. Part. Nucl. Phys. **120**, 103882 (2021)
60. J.J. Cowan, C. Sneden, J.E. Lawler et al., Origin of the heaviest elements: the rapid neutron-capture process. Rev. Mod. Phys. **93**, 015002 (2021)
61. M. Hausmann, F. Attallah, K. Beckert et al., First isochronous mass spectrometry at the experimental storage ring ESR. Nucl. Instrum. Meth. A. **446**, 569–580 (2000)
62. J. Stadlmann, M. Hausmann, F. Attallah et al., Direct mass measurement of bare short-lived ^{44}V, ^{48}Mn, ^{41}Ti and ^{45}Cr ions with isochronous mass spectrometry. Phys. Lett. B **586**, 27–32 (2004)
63. Y.H. Zhang, Y.A. Litvinov, T. Uesaka et al., Storage ring mass spectrometry for nuclear structure and astrophysics research. Phys. Scr. **91**, 073002 (2016)
64. H.F. Li, S. Naimi, T.M. Sprouse et al., First application of mass measurements with the rare-RI ring reveals the solar r-process abundance trend at A=122 and A=123. Phys. Rev. Lett. **128**, 152701 (2022)
65. H. Geissel, Y.A. Litvinov, Precision experiments with relativistic exotic nuclei at GSI. J. Phys. G: Nucl. Part. Phys. **31**, S1779 (2005)
66. H. Geissel, R. Knobel, Y.A. Litvinov et al., A new experimental approach for isochronous mass measurements of short-lived exotic nuclei with the FRS-ESR facility. Hyperfine Interact. **173**, 205–210 (2006)
67. B. Sun, R. Knobel, Y. Litvinov et al., Nuclear structure studies of short-lived neutron-rich nuclei with the novel large-scale isochronous mass spectrometry at the FRS-ESR facility. Nucl. Phys. A **812**, 1–12 (2008)
68. Y.M. Xing, M. Wang, Y.H. Zhang et al., First isochronous mass measurements with two time-of-flight detectors at CSRe. Phys. Scr. T **166**, 014010 (2015)
69. X. Zhou, M. Zhang, M. Wang et al., In-ring velocity measurement for isochronous mass spectrometry. Phys. Rev. Accel. Beams. **24**, 042802 (2021)
70. X.L. Yan, R.J. Chen, M. Wang et al., Characterization of a double time-of-flight detector system for accurate velocity measurement in a storage ring using laser beams. Nucl. Instrum. Meth. A. **931**, 52–59 (2019)
71. H. Sakaguchi, J. Zenihiro, Proton elastic scattering from stable and unstable nuclei- extraction of nuclear densities. Prog. Part. Nucl. Phys. **97**, 1–52 (2017)
72. W.H. Dickhoff, R.J. Charity, Recent developments for the optical model of nuclei. Prog. Part. Nucl. Phys. **105**, 252–299 (2019)
73. M. Mutterer, P. Egelhof, V. Eremin et al., Experimental techniques for in-ring reaction experiments. Phys. Scr. T **166**, 014053 (2015)
74. P. Egelhof, O. Kisselev, G. Munzenberg et al., Nuclear structure studies by direct reaction experiments with stored radioactive beams. Phys. Scr. T **104**, 151–159 (2003)
75. J. Glorius, C. Langer, Z. Slavkovska et al., Approaching the Gamow window with stored ions: direct measurement of ^{124}Xe (p, γ) in the ESR storage ring. Phys. Rev. Lett. **122**, 092701 (2019)
76. J.T. Zhang, K. Yue, H.X. Li et al., The development of in-ring reaction measurements at the HIRFL-CSR. Nucl. Instrum. Meth. A. **948**, 162848 (2019)
77. K. Yue, J.T. Zhang, X.L. Tu et al., Measurement of $^{58}Ni(p, p)^{58}Ni$ elastic scattering at low momentum transfer by using the HIRFL-CSR heavy-ion storage ring. Phys. Rev. C **100**, 054609 (2019)